Journal of Quantitative Spectroscopy & Radiative Transfer 251 (2020) 107086

Contents lists available at ScienceDirect

Journal of Quantitative Spectroscopy & Radiative Transfer

journal homepage: www.elsevier.com/locate/jqsrt

Spin-forbidden electronic transition properties of MgO

Tianrui Bai[a,b], Zhi Qin[a,b,c], Linhua Liu[a,b,*]

[a] School of Energy and Power Engineering, Shandong University, Jinan, Shandong, 250061, China
[b] Optics and Thermal Radiation Research Center, Shandong University, Qingdao, Shandong, 266237, China
[c] School of Energy Science and Engineering, Harbin Institute of Technology, Harbin 150001, China

ARTICLE INFO

Article history:
Received 5 March 2020
Revised 10 May 2020
Accepted 11 May 2020
Available online 22 May 2020

Keywords:
Spin-orbit coupling
Spin-forbidden transition
Franck-Condon factors
Radiative lifetimes

ABSTRACT

The spin-forbidden transitions of MgO are very important to the photodissociation dynamics and chemical reaction dynamics, which are frequently occurred in the interstellar space. In this work, the internally contracted multireference configuration interaction (icMRCI) method with the Davidson correction is used to compute the adiabatic potential energy curves (PECs) of eight Λ-S electronic states of MgO. Through considering the spin-orbit coupling (SOC) effect, the PECs of six splitting electronic states and the spin-forbidden transition dipole moments (TDMs) between the six lowest lying Ω states are also calculated. Using the calculated PECs and TDMs, the adiabatic transition parameters, including the Franck-Condon factors (FCFs) and radiative lifetimes for spin-forbidden transitions ($a^3\Pi_{0^+,1}-X^1\Sigma^+_{0^+}$ and $A^1\Pi_1-a^3\Pi_{0^+,1}$), are determined. As for the $a^3\Pi_{0^+,1}-X^1\Sigma^+_{0^+}$ transition, the radiative lifetimes are shorter, which means the stronger emission could occur. The FCFs for the $A^1\Pi_1-a^3\Pi_{0^+,1}$ transition are highly diagonal and the values are greater than 0.94, but with large vibrational radiative lifetimes. The results obtained in this work are consistent with experimental ones and can be used to further investigate the mechanism of chemical reaction dynamics.

1. Introduction

Magnesium oxide (MgO) is a major constituent of chondritic meteorites in the interstellar dust [1,2], and it has been detected in the lunar exosphere and Mercury in recent years [3]. Therefore, the determination of its spectral lines might help to yield the temperature and abundances in circumstellar environments.

MgO is also important for the application of target detection. For example, magnesium-based fuel scramjet has widely used all over the world because of the high energy density and "green" property of combustion products [4,5]. Especially, in the wake of the hypersonic vehicle, MgO exists in the high-temperature exhaust plume and is sprayed as an intermediate product of oxidation process. The spectrum of MgO can be analyzed to obtain the operational parameters of hypersonic vehicles. Therefore, it has been well recognized that the spectrum of MgO was a subject of many astrophysical observations and targets detection.

Given its contribution to astrophysics and target detection, previous works have established a series of experimental and theoretical studies to acquire the spectral transitions of MgO. For the experimental studies, a lot of spectrum bands were measured to improve the accuracy of molecular constants, such as, $B^1\Sigma^+$-$X^1\Sigma^+$ system, $B^1\Sigma^+$-$A^1\Pi$ system, $X^1\Sigma^+$-$A^1\Pi$ system, $D^1\Delta$-$A^1\Pi$ system, $d^3\Delta$-$a^3\Pi$ system, and so on [6–11]. Theoretically, a comprehensive calculation of MgO was carried out by Maatouk et al., who reported the potential energy curves, spectroscopic constants and spin-orbit couplings for the nine singlet and ten triplet lowest electronic states using the MRCI/cc-pV5Z method [12]. As a complement, the spin-allowed transition dipole moments and radiative lifetimes between the low-lying states were computed by Bauschlicher and Schwenke using SA-CASCF/MRCI/aug-cc-pV5Z method [13]. Meanwhile, the rovibration transitions within the low lying electronic states and other isotopologues were also investigated recently [14].

The rapid development of high-sensitivity spectrum-research techniques has provided more accurate information on the structures and spin-forbidden transitions between the low-lying states of MgO. For example, Mürtz et al. had observed the $A^1\Pi$- $X^1\Sigma^+$ bands and the much weaker $a^3\Pi$-$X^1\Sigma^+$ intercombination bands by Faraday laser magnetic resonance spectrometer[15, 16]. The spin-forbidden transitions between the other low-lying states of MgO, such as $B^1\Sigma^+$-$a^3\Pi$ system, $D^1\Delta$-$a^3\Pi$ system and $d^3\Delta$-$A^1\Pi$ system, had also been detected in previous measurements[8, 17]. The $A^1\Pi$ state and $a^3\Pi$ state as the two lowest excited states have drawn the attention of public because of spin–orbit and orbit–rotation interactions [18]. Especially, Kagi and Kawaguchi had

* Corresponding author.
E-mail address: liulinhua@sdu.edu.cn (L. Liu).

https://doi.org/10.1016/j.jqsrt.2020.107086
0022-4073/

discovered the pure rotational transitions in the $a^3\Pi_\Omega$ state in the 210-400 GHz region [19]. Nevertheless, the theoretical studies on spin-forbidden transition are still blank, only a few works focused on the TDMs for the $a^3\Pi_{0^+}-X^1\Sigma^+_{0^+}$ transition and $B^1\Sigma^+$ - $a^3\Pi$ transition had been done [20,21]. Although the transition probabilities for the$a^3\Pi_1-X^1\Sigma^+_{0^+}$,$a^3\Pi_{0^+}-X^1\Sigma^+_{0^+}$,$A^1\Pi_1-a^3\Pi_{0^+}$and $A^1\Pi_1$-$a^3\Pi_1$ transitions had been calculated in previous work, a one-particle basis was used to describe the wavefunctions and core-valence correlation and relativistic effect were still excluded [22]. This would lead to an inaccuracy result. Thus, it is urgent to obtain a more accurate and comprehensive theoretical investigation on a manifold of spin-forbidden transitions in the low-lying states of MgO.

In this work, the state-of-the-art *ab initio* methodology is applied to investigate the adiabatic spin-forbidden transitions of MgO. Firstly, the PECs of eight Λ-S states without SOC effect are calculated to obtain accurate spectroscopic parameters. Then, considering the SOC effect, the PECs and permanent dipole moments (PDMs) of the six lowest lying Ω states are calculated. Finally, the forbidden transition properties between six Ω states, including TDMs, FCFs and radiative lifetimes, are proposed in this work.

2. Computational details

Potential energy curves (PECs) of eight electronic states of MgO are carried out with MOLPRO procedure (version 2015) [23]. They are computed by the complete active space self-consistent field (CASSCF) method followed by the valence internally contracted MRCI approach with the Davidson correction (icMRCI+Q) [24–28]. To take into account of the the relativistic effect, the augmented correlation-consistent polarized core-valence quintuple-zeta basis set, aug-cc-pCV5Z-DK, coupled with the third-order Douglas–Kroll–Hess Hamiltonian is used in the computations [29–34]. Firstly, the PECs of eight Λ-S states are calculated without the spin-orbit coupling (SOC) effects. Next, to investigate the influence of SOC effects on the spin-forbidden transition, the state interaction method with Breit-Pauli Hamiltonian is used [35]. In the SOC calculations, the off-diagonal SO matrix elements are acquired from MRCI wave functions, where the diagonal elements are obtained from MRCI+Q calculations.

All the calculations in this work are carried out in C_{2v} group. Meanwhile, the electrons in the 1s and 2s2p shell of Mg and 1s and 2s shell of O are put into six closed-shell orbitals with four a_1 orbitals, one b_1 orbital and one b_2 orbital. The rest of electrons in the 3s shell of Mg and 2p shell of O are put into the active space. To improve the accuracy, two active spaces are considered in the calculations: active space 1 including nine molecular orbitals (MOs) and six outer electrons; active space 2 where one MO is added to active space 1.

The PECs, PDMs and TDMs are calculated over the internuclear range from 1.2 Å to 5.0 Å. According the results of PECs, rotational and centrifugal distortion constants for the vibrational levels of the low-lying electronic states of MgO are obtained via numerically solving the one-dimensional Schrödinger equation of nuclear motion with the LEVEL 8.0 program package [36]. The vibrational constant (ω_e and $\omega_e\chi_e$) and rotational constant (B_e and α_e) are determined by the calculated vibrational level energy (G_v) and inertial rotational constant (B_v) at each vibrational quantum number v, and they can be expanded as

$$G_v = \sum_{l=1}^{n} Y_{l,0}\left(v+\frac{1}{2}\right) = \omega_e\left(v+\frac{1}{2}\right) - \omega_e\chi_e\left(v+\frac{1}{2}\right)^2 + \cdots \quad (1)$$

$$B_v = \sum_{l=1}^{n} Y_{l,1}\left(v+\frac{1}{2}\right)^l = B_e - \alpha_e\left(v+\frac{1}{2}\right) + \cdots . \quad (2)$$

where $Y_{l,0}$ and $Y_{l,1}$ are Dunham coefficients.

Based on the PECs and TDMs, the Franck-Condon factors and radiative lifetimes for the transitions at different vibrational levels are also determined via solving the nuclear Schrödinger equation. A concrete solution method can refer to previous publications in our group [37,38].

3. Results and discussions

3.1. Potential energy curves and spectroscopic parameters

In the present work, eight Λ-S electronic states, including $X^1\Sigma^+$, $A^1\Pi$, $D^1\Delta$, $B^1\Sigma^+$, $a^3\Pi$, $b^3\Sigma^+$, $c^3\Sigma^+$ and $d^3\Delta$, are characterized theoretically. The PECs versus the internuclear distances are shown in Fig. 1. The states correlate to the first three dissociation limits and the relative energies for these dissociation limits are listed in Table 1. Comparing with the experimental values, the energy separations between the first, second and third dissociation limits are in good agreement [37]. As shown in Fig. 1, the $X^1\Sigma^+$ state is crossed by the $a^3\Pi$ state and $A^1\Pi$ state at around 2.0 and 2.1 Å, respectively. Meanwhile, the $D^1\Delta$, $d^3\Delta$ and $c^3\Sigma^+$ states are also strongly mixed for energies above 27000 cm^{-1}. It is beneficial to the interactions between these states through spin-orbit and rotational and vibronic couplings.

According to our PECs, the spectroscopic parameters of eight Λ-S states, including adiabatic excitation energy (T_e), equilibrium internuclear distance (R_e), vibrational constant (ω_e and $\omega_e\chi_e$) and rotational constant (B_e and α_e), are calculated by solving the Schrödinger equation of nuclear motion and shown in Table 2. The main electron configurations of eight states near the corresponding equilibrium internuclear distances are also calculated and descripted in Table 3 to investigate the transition properties. Comparing with the previous experiments, except the $b^3\Sigma^+$state, all the others have been detected. The corresponding spectroscopic parameters are consistent with the earlier experimental and theoretical results. For the singlet states, the results using the active

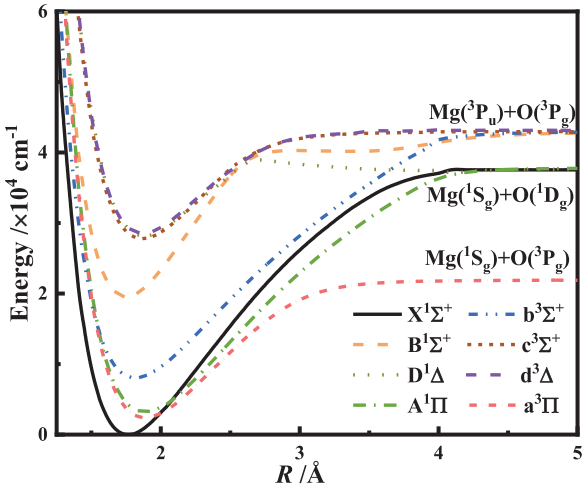

Fig. 1. The potential energy of eight Λ-S electronic states of MgO calculated at the icMRCI/aug-cc- pCV5Z-DK level of theory.

Table 1
Dissociation relationships of eight Λ-S states of MgO.

Atomic states	Λ-S Electronic state	Relative energy/cm^{-1}	
		This work	Exp. [39]
Mg (^1S_g) + O (^3P_g)	$a^3\Pi$	0.00	0.00
Mg (^1S_g) + O (^1D_g)	$X^1\Sigma^+$, $A^1\Pi$, $D^1\Delta$	15830.881	15867.862
Mg (^3P_u) + O (^3P_g)	$B^1\Sigma^+$, $d^3\Delta$, $b^3\Sigma^+$, $c^3\Sigma^+$	21057.998	21850.405

Table 2
Spectroscopic parameters of eight electronic states of MgO obtained by the icMRCI+Q/aug-cc-pCV5Z-DK method.

State		T_e/cm^{-1}	R_e/Å	ω_e/cm^{-1}	$\omega_e x_e$/cm^{-1}	B_e/cm^{-1}	$10^3\alpha_e$/cm^{-1}
$X^1\Sigma^+$	This work[a]	0	1.763	781.7	9.44	0.5670	6.90
	This work[b]	0	1.763	772.32	6.44	0.5650	5.14
	Cal. [12]	0	1.766	769.0	4.45	0.5314	5.13
	Cal. [40]	0	1.751	781.80			
	Exp. [41]	0	1.749	785.06	5.18	0.5743	5.00
	Exp. [11]	0		785.22	5.13	0.5748	5.32
	Exp. [19]	0		785.26	5.12	0.5748	5.33
$a^3\Pi$	This work[b]	2376.8	1.885	641.7	8.20	0.4960	7.73
	Cal. [12]	1645.4	1.885	644.8	5.3	0.494	4.24
	Cal. [40]	2480.9	1.872	646.0			
	Exp. [41]	2400	1.870	650.2	4.2	0.502	5.34
	Exp. [19]	2618.95		650.18	4.2	0.5027	4.67
	Exp. [17]	2620.6	1.869	650.2	4.2	0.503	5.34
$A^1\Pi$	This work[a]	3074.0	1.902	662.0	14.19	0.4903	1.51
	This work[b]	3216.1	1.882	662.29	15.68	0.4954	1.71
	Cal. [12]	3078.5	1.879	654.3	4.03	0.498	4.24
	Cal. [13]	2811	1.879	660.0			
	Exp. [19]	3558.5		664.44	3.93	0.5054	4.66
	Exp. [17]	3560.1	1.863	664.3	3.8	0.505	4.69
$b^3\Sigma^+$	This work[b]	8026.6	1.811	670.1	7.90	0.5330	5.41
	Cal. [1]	7726.6	1.807	673.7	4.37	0.5378	5.33
	Cal. [42]	8414	1.863	616		0.505	
$B^1\Sigma^+$	This work[a]	19683.3	1.749	810.0	8.93	0.5764	8.80
	This work[b]	19549.9	1.752	804.2	4.06	0.5724	4.72
	Cal. [12]	19332.7	1.753	808.2	3.75	0.571	4.81
	Exp. [41]	19984.0	1.737	824.08	4.76	0.582	4.50
$c^3\Sigma^+$	This work[b]	27786.0	1.868	660.5	4.07	0.5042	4.87
	Cal. [12]	27703.0	1.880	642.4	4.60	0.4968	4.95
	Exp. [41]	28300					
$d^3\Delta$	This work[b]	28527.0	1.872	653.6	3.73	0.5023	5.26
	Cal. [12]	28930.5	1.875	653.5	4.34	0.499	4.78
	Exp. [8]	29466.2	1.871	655.2	4.9	0.507	5.34
	Exp.[41]	29300	1.870	650		0.50	
$D^1\Delta$	This work[a]	29033.6	1.877	642.7	7.13	0.4955	5.88
	This work[b]	28911.5	1.872	657.94	3.11	0.5013	6.34
	Cal. [12]	29228.2	1.886	625.1	4.27	0.494	5.46
	Exp. [8]	29835.5	1.861	631.6	5.2	0.501	5.45
	Exp. [41]	29851.6	1.872	632.5	5.3	0.501	4.8

[a] calculated by the active space 1 including nine molecular orbitals and six outer electrons with five a_1 orbitals, two b_1 orbitals and two b_2 orbitals.
[b] calculated by the active space 2 where one MO is added to active space 1.

Table 3
Main electron configurations near the corresponding equilibrium internuclear distances.

State	Main electron configuration	State	Main electron configuration
$X^1\Sigma^+$	$6\sigma^2 7\sigma^0 2\pi^4 3\pi^0$(0.33)	$a^3\Pi$	$6\sigma^2 7\sigma^1 2\pi^3 3\pi^0$ (0.66)
	$6\sigma^1 7\sigma^1 2\pi^4 3\pi^0$ (0.27)		
$A^1\Pi$	$6\sigma^2 7\sigma^1 2\pi^3 3\pi^0$(0.62)	$b^3\Sigma^+$	$6\sigma^1 7\sigma^1 2\pi^4 3\pi^0$ (0.68)
	$6\sigma^2 8\sigma^1 2\pi^3 3\pi^0$(0.14)		$6\sigma^1 8\sigma^1 2\pi^4 3\pi^0$ (0.15)
$B^1\Sigma^+$	$6\sigma^2 7\sigma^0 2\pi^3 3\pi^1$ (0.30)	$c^3\Sigma^+$	$6\sigma^2 7\sigma^0 2\pi^3 3\pi^1$ (0.79)
	$6\sigma^1 7\sigma^1 2\pi^4 3\pi^0$ (0.28)		
	$6\sigma^2 7\sigma^0 2\pi^4 3\pi^0$ (0.17)		
$D^1\Delta$	$6\sigma^2 7\sigma^0 2\pi^3 3\pi^1$(0.74)	$d^3\Delta$	$6\sigma^2 7\sigma^0 2\pi^3 3\pi^1$ (0.87)

space 1 are more close to the experimental values than those from Maatouk et al. [12]. It is attributed to the scalar relativistic correction and diffuse functions for description of weak interactions in the calculations.

As we have aforementioned, the $X^1\Sigma^+$, $A^1\Pi$ and $a^3\Pi$ states are of interest. For the ground state, the calculated equilibrium bond distance R_e is 1.763 Å and the corresponding difference is 0.014 Å with respect to the experiment value. Meanwhile, the ω_e is extremely close to the experimental value of 785.06 cm^{-1} and the theoretical value of 781.8 cm^{-1} calculated by RCCSD(T)/aug-cc-pCV5Z method [40]. Moreover, the value of B_e = 0.5670 cm^{-1} is also in good agreement with the experiment data of 0.5743 cm^{-1}. For the $a^3\Pi$ state, T_e = 2376.84 cm^{-1} is close to the value of Huber et al. [41], but smaller than that of Kagi et al. [19] and Ip et al. [17]. Additionally, the calculated ω_e and R_e are 641.7 cm^{-1} and 1.885 Å, respectively, which well reproduce the experimental results with a deviation of 8.5 cm^{-1} and 0.015 Å. For the $A^1\Pi$ state, the values obtained by using active space 2 are much closer to the experimental data. The corresponding deviations of ω_e and R_e are only 2 cm^{-1}and 0.019 Å, respectively.

The three lowest lying electronic states ($X^1\Sigma^+$, $a^3\Pi$ and $A^1\Pi$) are strongly mixed by rotational or spin-orbit couplings, which plays an important role in investigating the energy splitting and spin-forbidden transition. After considering the SOC effect, there are six low-lying Ω states generated from the above three Λ-S states, and the corresponding PECs are shown in Fig. 2. Based on the PECs, the spectroscopic parameters of the six Ω states could be calculated, as shown in Table 4. However, only the $a^3\Pi_2$ state have been measured via the experimental study by Bellert et al., where the rotational (B_e = 0.496 cm^{-1}, α_e = 0.005 cm^{-1}) and vibrational (ω_e = 649.1 cm^{-1}, $\omega_e x_e$ = 4.0 cm^{-1}) spectroscopic constants have been observed [43]. Comparing with the experimental results, the calculated ω_e = 642.39 cm^{-1} is smaller but B_e = 0.494 cm^{-1} is similar to the experimental value. It implies our calculated results are available and could be used for the further calculation.

3.2. Spin-forbidden transition properties between the $X^1\Sigma^+$, $a^3\Pi$ and $A^1\Pi$ states

The spin-forbidden transitions between the $X^1\Sigma^+$, $a^3\Pi$ and $A^1\Pi$ states would happen after the consideration of the SOC effect. Firstly, the permanent dipole moments (PDMs) of the$X^1\Sigma^+_{0^+}$,

Table 4
Spectroscopic parameters of the six lowest Ω states of the MgO molecule.

State		T_e/cm^{-1}	R_e/Å	ω_e/cm^{-1}	$\omega_e x_e$/cm^{-1}	B_e/cm^{-1}	$10^3\alpha_e$/cm^{-1}
$X^1\Sigma^+_{0^+}$	This work	0	1.751	778.62	4.89	0.5677	7.39
$a^3\Pi_2$	This work	2346.59	1.885	642.39	5.21	0.4941	3.64
	Exp. [43]			649.1	4.0	0.496	5.0
$a^3\Pi_1$	This work	2404.73	1.884	650.55	15.70	0.4937	2.05
$a^3\Pi_{0^-}$	This work	2471.84	1.884	644.43	12.60	0.4935	2.26
$a^3\Pi_{0^+}$	This work	2476.17	1.884	647.01	15.15	0.4955	6.71
$A^1\Pi_1$	This work	3243.19	1.881	639.92	3.29	0.4941	4.21

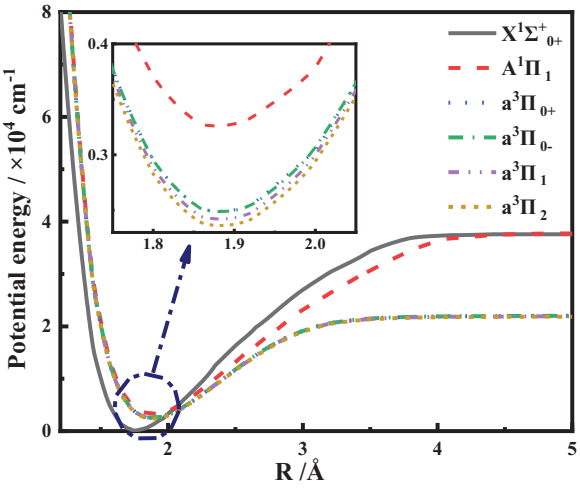

Fig. 2. PECs of the six lowest Ω states of the MgO molecule.

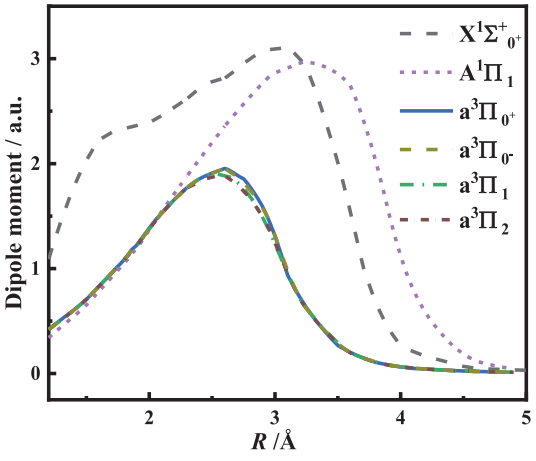

Fig. 3. Dipole moments of the low-lying six Ω states.

$A^1\Pi_1$,$a^3\Pi_{0^+}$,$a^3\Pi_{0^-}$,$a^3\Pi_1$and $a^3\Pi_2$ states are calculated, which are a function of the internuclear distance and displayed in Fig. 3. The PDMs of all electronic states tend to zero in the large internuclear distance, indicating that their dissociation products are neutral atoms, which is consistent with the theoretical derivation of the dissociation limit. The calculated dipole moment of $X^1\Sigma^+_{0^+}$ is 2.35 a.u. for the vibrational level $\upsilon = 0$, which is close to the experimental value of $\mu_{v=0} = 2.44$ a.u.$\mu_{v=0}$= 2. a.u. [44]. The main electron configurations of $X^1\Sigma^+_{0^+}$ are $6\sigma^2 7\sigma^0 2\pi^4 3\pi^0$ and $6\sigma^1 7\sigma^1 2\pi^4 3\pi^0$ near the equilibrium internuclear distance. It indicates the ground state is strong polar and the electrons in 3s shell of Mg are transferred into 2p shell of O in the process of molecular formation. Obviously, as shown in Fig. 3, the PDMs of

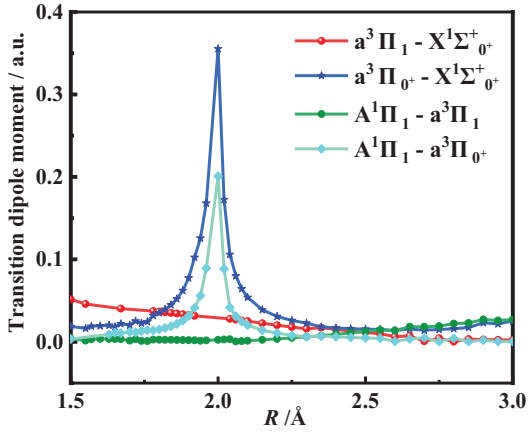

Fig. 4. Transition dipole moments of the $a^3\Pi_1$–$X^1\Sigma^+_{0^+}$, $a^3\Pi_{0^+}$–$X^1\Sigma^+_{0^+}$, $A^1\Pi_1$–$a^3\Pi_{0^+}$and $A^1\Pi_1$-$a^3\Pi_1$ transitions.

the $a^3\Pi_i$ (I = 0^+, 0^-,1,2) state and $A^1\Pi_1$ state are close near the equilibrium internuclear distances, and they are also lower than those of the $X^1\Sigma^+_{0^+}$ state. It is due to the similar electron configurations ($6\sigma^2 7\sigma^1 2\pi^3 3\pi^0$ and $6\sigma^2 8\sigma^1 2\pi^3 3\pi^0$) and weaker polarity of the $a^3\Pi$ state and $A^1\Pi$ state.

According to the transition selection rule, the$a^3\Pi_1$–$X^1\Sigma^+_{0^+}$,$a^3\Pi_{0^+}$–$X^1\Sigma^+_{0^+}$,$A^1\Pi_1$–$a^3\Pi_{0^+}$, $A^1\Pi_1$-$a^3\Pi_1$, $A^1\Pi_1$-$a^3\Pi_2$and$A^1\Pi_1$–$a^3\Pi_{0^-}$transitions are allowed, the corresponding adiabatic transition dipole moments (TDMs) are also calculated. However, TDMs for $A^1\Pi_1$-$a^3\Pi_2$ and $A^1\Pi_1$–$a^3\Pi_{0^-}$ transitions are too small near the equilibrium internuclear distances (1.5–3 Å). Thus, for the sake of visual clarity, only the other four spin-forbidden transitions are plotted in Fig. 4. Comparing with the previous works, the calculated TDMs for $a^3\Pi_{0^+}$–$X^1\Sigma^+_{0^+}$are larger than the results proposed by Thümmel et al. [42]. For example, the TDMs are calculated by Thümmel et al. to 0.0076, 0.0051, 0.0039, 0.0030, 0.0024 a.u. at the different internuclear distances R = 1.6, 1.7, 1.8, 1.9, 2.0 Å, respectively. It is attributed to a one-particle basis used by Thümmel et al. to describe the wavefunctions, which also neglect the relativistic effect. In theory, the state-of-the-art *ab initio* methodology and basis set are used in our work, which is conductive to get a more reliable result. Nevertheless, it still needs further experimental study to verify the results obtained in this work. Besides, when we calculated the spin-orbit TDMs, we considered the contribution from quasidegenerate space, not including outside the quasidegenerate space, which can be solved by referring to the procedure proposed by DeVivie et al.[45] and an application by Yarkony [22].

For the $a^3\Pi_1 - X^1\Sigma^+_{0^+}$ transition, the curve shows a linear approximation and drops gradually to zero. In contrast, the TDMs of $A^1\Pi_1$-$a^3\Pi_1$ transition exhibits an opposite tendency, which increases from zero to 0.0289 a.u. As for the $a^3\Pi_{0^+}$–$X^1\Sigma^+_{0^+}$ and $A^1\Pi_1$–$a^3\Pi_{0^+}$ transitions, the spikes appear and the peak values

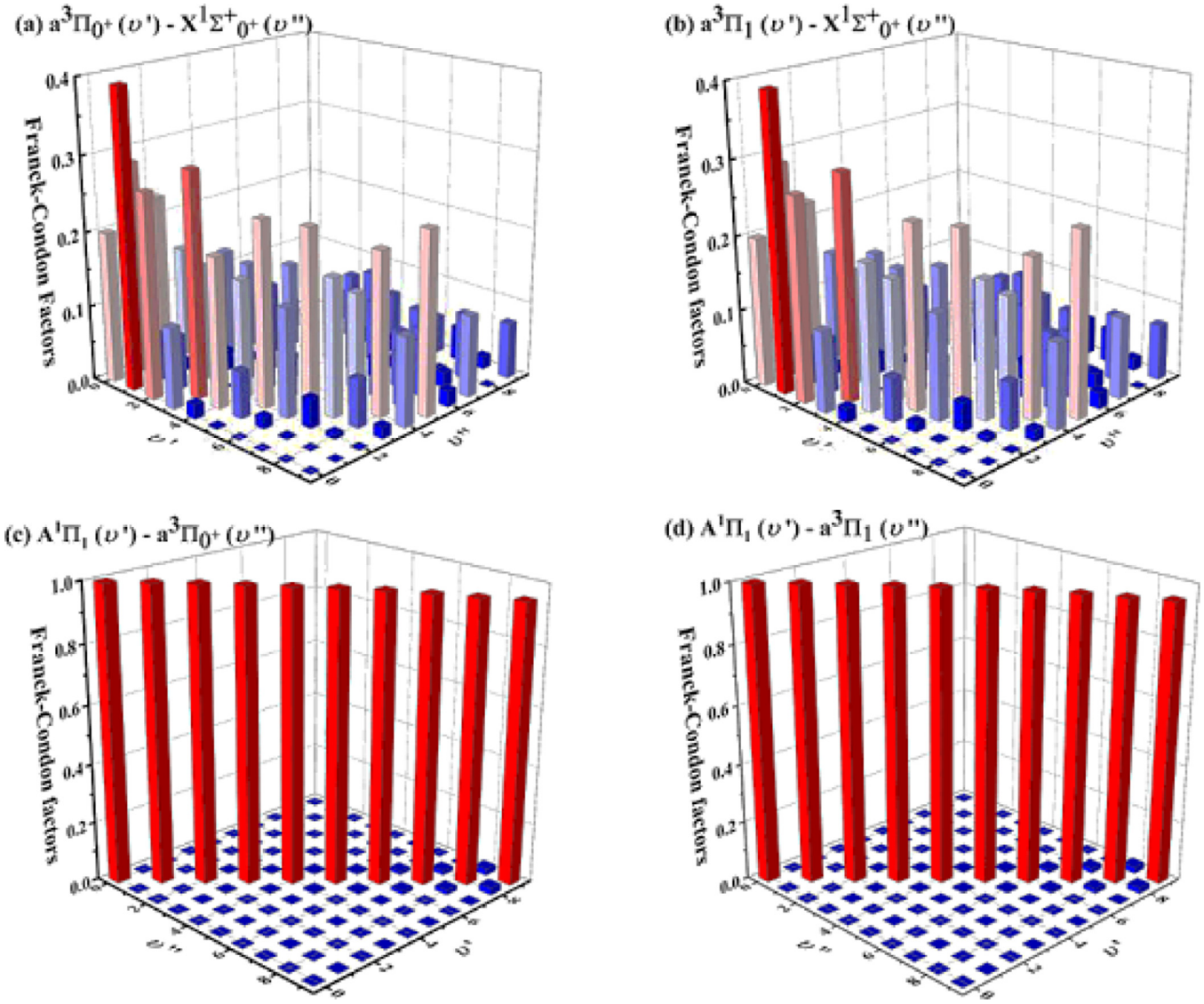

Fig. 5. Franck-Condon factors for the $a^3\Pi_1-X^1\Sigma^+_{0^+}$,$a^3\Pi_{0^+}-X^1\Sigma^+_{0^+}$,$A^1\Pi_1-a^3\Pi_{0^+}$ and $A^1\Pi_1$-$a^3\Pi_1$ transitions.

at about 2.0 Å are 0.3554 a.u. and 0.2010 a.u., respectively. It is attributed to the non-adiabatic couplings and the invalidation of Born-Oppenheimer approximation, when they are close in energy. However, the non-adiabatic effect is not considered in present work. In the near future, we will compute non-adiabatic couplings between these electronic states.

Based on the standard second-order perturbation theory including spin-orbit, orbit-rotation and Zeeman interactions, the perturbative contribution to the above transitions has been investigated [10,15,16,20]. For the perturbation of between the $a^3\Pi$ state and $X^1\Sigma^+$ state, the higher lying levels such as $\upsilon = 2, 3, 4$ of the $a^3\Pi_1$ state are equally perturbed and those of the $a^3\Pi_0$ state are more strongly perturbed, which is consistent with our calculated result that TDMs for the $a^3\Pi_0$ -$X^1\Sigma^+$ transition is greater. Besides, with the contribution of the spin-spin interaction in the $a^3\Pi$ state, the other higher lying electronic states ($b^3\Sigma^+$, $B^1\Sigma^+$) also show the direct influence [15,16]. As for the $A^1\Pi$ state and $a^3\Pi$ state, the spectroscopic constants are similar, and the eigenvectors of the $a^3\Pi$ state show that the strongest perturbation comes from each level of the $A^1\Pi$ state [20].

To further describe the transition probabilities between the $X^1\Sigma^+$, $a^3\Pi$ and $A^1\Pi$ states, FCFs and radiative lifetimes can be used. FCFs are determined by the degree of overlap for vibrational wave functions. Based on the PECs and TDMs, FCFs and radiative lifetimes are calculated of different vibrational levels for the $a^3\Pi_1-X^1\Sigma^+_{0^+}$,$a^3\Pi_{0^+}-X^1\Sigma^+_{0^+}$, $A^1\Pi_1-a^3\Pi_{0^+}$ and$A^1\Pi_1$-$a^3\Pi_1$ transitions, which are displayed in Fig. 5 and Table 5, respectively. As shown in Fig. 5, the distributions of FCFs of $a^3\Pi_i-X^1\Sigma^+_{0^+}$ and

Table 5
Radiative lifetimes (s) of the $a^3\Pi_1-X^1\Sigma^+_{0^+}$,$a^3\Pi_{0^+}-X^1\Sigma^+_{0^+}$,$A^1\Pi_1-a^3\Pi_{0^+}$ and $A^1\Pi_1$-$a^3\Pi_1$ transitions.

υ'	$a^3\Pi_1-X^1\Sigma^+_{0^+}$	$a^3\Pi_{0^+}-X^1\Sigma^+_{0^+}$	$A^1\Pi_1-a^3\Pi_{0^+}$	$A^1\Pi_1$-$a^3\Pi_1$
0	0.3485	0.0163	0.1165	790.5293
1	0.2199	0.0050	0.0474	228.6149
2	0.1171	0.0039	0.0939	166.1805
3	0.0972	0.0117	0.3109	719.3597
4	0.0790	0.0078	0.1516	1399.6330
5	0.0796	0.0141	0.6459	1013.1626
6	0.1180	0.0629	0.0954	1213.2933
7	0.0933	0.0658	0.4712	272.0002
8	0.0803	0.1958	0.0531	382.3523
9	0.0673	0.2207	0.2400	109.8559

$A^1\Pi_1$-$a^3\Pi_i$ transitions are very similar. It is ascribed to the similar PECs of $a^3\Pi_{0^+}$and $a^3\Pi_1$ states.

For the $a^3\Pi_{0^+}-X^1\Sigma^+_{0^+}$ and $a^3\Pi_1-X^1\Sigma^+_{0^+}$ transitions, the maximum values of FCFs are similar and occur at the (0, 1) vibrational band, which are 0.3967 and 0.3973, respectively. It indicates the high line intensity would be observed. As Mürtz et al. measured the $a^3\Pi_{0,1}$ - $X^1\Sigma^+$ transition with the CO laser in the 1640-1970 cm^{-1}, they could not detect transitions involving higher levels with $\upsilon' > 1$ of the $a^3\Pi$ state [16]. As shown in Fig. 4, the TDMs for the $a^3\Pi_{0^+}-X^1\Sigma^+_{0^+}$ transition are relatively larger, which would lead to the smaller radiative lifetimes and stronger emission. For example, the radiative lifetimes for the $a^3\Pi_{0^+}-X^1\Sigma^+_{0^+}$ transition are calculated to 0.0163, 0.0050, 0.0039, 0.0117 and 0.0078 s at the vibrational levels $\upsilon' = 0, 1, 2, 3, 4$, respectively. The results are consistent with the experiments from Mürtz et al. and calculations from Thümmel et al., which indicate the higher lying levels such as $\upsilon' = 2, 3, 4$ of $a^3\Pi_{0^+}$ state are more strongly perturbed than those of $a^3\Pi_1$ state [16,22]. All evidence is that our results give a reliable description for the $a^3\Pi_i$ - $X^1\Sigma^+$ transition.

For the $A^1\Pi_1$-$a^3\Pi_i$ transition, the equilibrium position of the $A^1\Pi$ and $a^3\Pi$ states are so similar that the calculated FCFs are highly diagonal and greater than 0.9488 ($\upsilon' = 0$–9). However, the radiative lifetimes for the $A^1\Pi_1$-$a^3\Pi_1$ transition are too long because of small TDMs near equilibrium position, which are calculated and displayed in Table 5. For the $A^1\Pi_1-a^3\Pi_{0^+}$ transition at different vibrational levels, the radiative lifetimes are much smaller, implying a stronger emission of the $A^1\Pi_1-a^3\Pi_{0^+}$ transition compared with the $A^1\Pi_1$-$a^3\Pi_1$ transition. Up to now, there have been no experiments for the $A^1\Pi_1$-$a^3\Pi_i$ transition, only the perturbation between $A^1\Pi$ state and $a^3\Pi$ state has been investigated in the previous literatures [10,12,16]. To have a better knowledge of the transition properties, the experiments using high-sensitivity spectrum-research techniques are required.

In order to further study the transition mechanism, the process of electron transition is also analyzed. As shown in Table 3, the calculated electron configurations of the ground state ($X^1\Sigma^+$) near the equilibrium internucler distance are $6\sigma^2 7\sigma^0 2\pi^4 3\pi^0$ (0.33) and $6\sigma^1 7\sigma^1 2\pi^4 3\pi^0$ (0.27). Moreover, the $a^3\Pi$ state is mainly characterized by $6\sigma^2 7\sigma^1 2\pi^3 3\pi^0$ (0.66). Hence, it is formed by the $2\pi \rightarrow 7\sigma/6\sigma$ electron excitation. For the $A^1\Pi_1$-$a^3\Pi_i$ transition, the $A^1\Pi$ and $a^3\Pi$ states have the same electron configurations ($6\sigma^2 7\sigma^1 2\pi^3 3\pi^0$ and $6\sigma^2 8\sigma^1 2\pi^3 3\pi^0$) near their equilibrium internucler distance, which indicates that there exist many transitions in this system.

4. Conclusion

In this work, the state-of-the-art *ab initio* methodology at the icMRCI /aug-cc-pCV5Z-DK level of theroy is used to investigate adiabatic spin-forbidden transition prosperties for the low-lying electronic states of MgO. Firstly, the PECs of eight Λ-S states without SOC effect and six lowest lying Ω states with SOC effect are calculated. Next, according to the PECs of eight Λ-S states, the calculated spectroscopic parameters (R_e, ω_e, $\omega_e x_e$, B_e and T_e) are in good agreement with the available theoretical and experimental values. But as for the splitting states, only $a^3\Pi_2$ state has the experimental parameters, which are also close to our calculated ones.

Subsequently, the spin-forbidden transition properties between six lowest lying Ω states ($X^1\Sigma^+_{0^+}$,$A^1\Pi_1$, $a^3\Pi_{0^+}$,$a^3\Pi_{0^-}$,$a^3\Pi_1$,$a^3\Pi_2$) are invesitigated. At the first step, the PDMs and TDMs versus the internuclear distances are obtained. Based on the PECs and TDMs, the FCFs and radiative lifetimes of the different vibrational levels are calculated by the LEVEL 8.0 program package for the $a^3\Pi_1-X^1\Sigma^+_{0^+}$,$a^3\Pi_{0^+}-X^1\Sigma^+_{0^+}$, $A^1\Pi_1-a^3\Pi_{0^+}$ and $A^1\Pi_1$-$a^3\Pi_1$ transitions. For the $a^3\Pi_i-X^1\Sigma^+_{0^+}$ transition, the maximum value of FCFs occurs at the (0 - 1) vibrational band, which indicates the high line intensity would be observed. Due to larger TMDs for the $a^3\Pi_{0^+}-X^1\Sigma^+_{0^+}$ transition, the radiative lifetimes are smaller, which are consistent with the other experiments and calculations. The calculated FCFs of the $A^1\Pi_1$-$a^3\Pi_i$ (i =0^+, 1) transition are highly diagonal and greater than 0.9488 because of the similar equilibrium position of the $A^1\Pi$ state and $a^3\Pi$ state. However, the radiative lifetimes are too long due to the small TDMs near the equilibrium position. So far, no experiments for the $A^1\Pi_1$-$a^3\Pi_i$ transition have been done and further experimental study to verify the results obtained in this work is required. Additionally, the results in this paper are based on Born-Oppenheimer approximation, leading to inaccurate calculations when the states are close in energy. In the near future, we will compute diabatization calculation that includes spin-orbit coupling.

Supplementary material

Supplementary material associated with this article can be found in the document named“Supplementary material”.

Declaration of Competing Interest

The authors declare that they have no known competing financial interests or personal relationships that could have appeared to influence the work reported in this paper.

CRediT authorship contribution statement

Tianrui Bai: Software, Investigation, Conceptualization, Methodology, Writing - original draft. **Zhi Qin:** Investigation, Conceptualization, Software, Methodology, Writing - review & editing. **Linhua Liu:** Supervision, Funding acquisition, Conceptualization, Writing - review & editing.

Ackonowledgements

This work is sponsored by the National Natural Science Foundation of China under Grant nos. 51336002, 51421063.

Supplementary materials

Supplementary material associated with this article can be found, in the online version, at doi:10.1016/j.jqsrt.2020.107086.

References

[1] Plane JM. Atmospheric chemistry of meteoric metals. Chem Rev 2003;103:4963–84.
[2] Sarantos M, Killen RM, McClintock WE, Bradley ET, Vervack RJ Jr, Benna M, et al. Limits to Mercury's magnesium exosphere from MESSENGER second flyby observations. Planet Space Sci 2011;59:1992–2003.
[3] Berezhnoy A, Churyumov K, Kleshchenok V, Kozlova E, Mangano V, Pakhomov YV, et al. Properties of the lunar exosphere during the Perseid 2009 meteor shower. Planet Space Sci 2014;96:90–8.
[4] Yang Y, He M. Numerical study on operating characteristics of a magnesium-based fuel ramjet. Acta Astronautica 2012;79:96–106.
[5] Sandall E, Kalman J, Quigley JN, Munro S, Hedman TD. A study of solid ramjet fuel containing boron–magnesium mixtures. Propuls Power Res 2017;6:243–52.
[6] Dreyer CB, Daily JW, Abbud-Madrid A, Branch MC. Laser-induced fluorescence excitation spectroscopy of the magnesium oxide $B^1\Sigma^+$–$A^1\Pi$ system. Appl Opt 2001;40:2561–70.
[7] Kagi E, Hirano T, Takano S, Kawaguchi K. Fourier transform infrared spectroscopy of the $A^1\Pi$-$X^1\Sigma^+$ System of MgO. J Mol Spectrosc 1994;168:109–25.
[8] Bourguignon B, Rostas J. The $d^3\Delta_i$-$a^3\Pi_i$ and $d^3\Delta_2$-$A^1\Pi$ systems of the MgO molecule. J Mol Spectrosc 1991;146:437–54.
[9] Stojadinović S, Perić M, Radić-Perić J, Vasilić R, Petković M, Zeković L. Luminescence of the $B^1\Sigma^+$–$X^1\Sigma^+$ band system of MgO during plasma electrolytic oxidation of magnesium alloy. Surface Coat Technol 2012;206:2905–13.
[10] Ikeda T, Wong NB, Harris DO, Field RW. Argon ion and dye laser induced MgO $B^1\Sigma^+$-$X^1\Sigma^+$ and $B^1\Sigma^+$-$A^1\Pi$ photoluminescence spectra: analysis of $a^3\Pi_i$~$X^1\Sigma^+$ perturbations. J Mol Spectrosc 1977;68:452–87.

[11] Daily JW, Dreyer C, Abbud-Madrid A, Branch MC. Transition probabilities in the $B^1\Sigma^+$–$X^1\Sigma^+$ and the $B^1\Sigma^+$–$A^1\Pi$ electronic systems of MgO. J Mol Spectrosc 2002;214:111–16.
[12] Maatouk A, Ben Houria A, Yazidi O, Jaidane N, Hochlaf M. Electronic states of MgO: spectroscopy, predissociation, and cold atomic Mg and O production. J Chem Phys 2010;133:144302.
[13] Bauschlicher CW Jr, Schwenke DW. The low-lying electronic states of MgO. Chem Phys Lett 2017;683:62–7.
[14] Li HY, Tennyson J, Yurchenko SN. ExoMol line lists–XXXII. The rovibronic spectrum of MgO. Mon Not R Astron Soc 2019;486:2351–65.
[15] Mürtz P, Richter S, Pfelzer C, Thümmel H, Urban W. Faraday LMR spectroscopy of the MgO $A^1\Pi-X^1\Sigma^+(0–2)$ and $a^3\Pi_{0,1}-X^1\Sigma^+(0–1)$ bands. Mol Phys 1994;82:989–1007.
[16] Mürtz P, Thümmel H, Pfelzer C, Urban W. New bands of the MgO $A^1\Pi$–$X^1\Sigma^+$ and $a^3\Pi_{0,1}$-$X^1\Sigma^+$ systems by Faraday laser magnetic resonance spectroscopy. Mol Phys 1995;86:513–34.
[17] Ip P, Cross K, Field R, Rostas J, Bourguignon B, McCombie J. The $B^1\Sigma^+$-$a^3\Pi_i$ and $D^1\Delta$-$a^3\Pi_1$ intercombination systems of the MgO molecule. J Mol Spectrosc 1991;146:409–36.
[18] Kim JH, Li X, Wang L-S, de Clercq HL, Fancher CA, Thomas OC, et al. Vibrationally resolved photoelectron spectroscopy of $MgO^-$and $ZnO^-$and the low-lying electronic states of MgO, MgO^-, and ZnO. J Phys Chem A 2001;105:5709–18.
[19] Kagi E, Kawaguchi K. Microwave spectroscopy of MgO in the $a^3\Pi$ and $X^1\Sigma^+$ states. J Mol Struct 2006;795:179–84.
[20] Yarkony DR. Spin-forbidden radiative decay involving quasidegenerate states. Application to the $B^1\Sigma^+ \rightarrow a\ ^3\Pi$ transition in MgO. J Chem Phys 1988;89:7324–33.
[21] Matsui M. Molecular dynamics study of the structural and thermodynamic properties of MgO crystal with quantum correction. J Chem Phys 1989;91:489–94.
[22] Thümmel H, Klotz R, Peyerimhoff SD. The electronic structure of the MgO molecule in ground and excited states. Chem Phys 1989;129:417–30.
[23] Werner H, Knowles P, Knizia G, Manby F, Schütz M, Celani P, et al. Molpro, Version 2015.1, A Package of Ab Initio Programs. Cardiff, UK. 2015.
[24] Knowles PJ, Werner H-J. An efficient second-order MC SCF method for long configuration expansions. Chem Phys Lett 1985;115:259–67.
[25] Werner HJ, Knowles PJ. A second order multiconfiguration SCF procedure with optimum convergence. J Chem Phys 1985;82:5053–63.
[26] Knowles PJ, Werner H-J. An efficient method for the evaluation of coupling coefficients in configuration interaction calculations. Chem Phys Lett 1988;145:514–22.
[27] Werner HJ, Knowles PJ. An efficient internally contracted multiconfiguration–reference configuration interaction method. J Chem. Phys 1988;89:5803–14.
[28] Qin Z, Zhao J, Liu L. Energy levels, transition dipole moment, transition probabilities and radiative lifetimes for low-lying electronic states of PN. J Quant Spectrosc Radiat Transfer 2019;227:47–56.
[29] Dunning TH Jr. Gaussian basis sets for use in correlated molecular calculations. I. The atoms boron through neon and hydrogen. J Chem Phys 1989;90:1007–23.
[30] Kendall RA, Dunning TH Jr, Harrison RJ. Electron affinities of the first-row atoms revisited. Systematic basis sets and wave functions. J Chem Phys 1992;96:6796–806.
[31] Woon DE, Dunning TH Jr. Gaussian basis sets for use in correlated molecular calculations. III. The atoms aluminum through argon. J Chem Phys 1993;98:1358–71.
[32] Woon DE, Dunning TH Jr. Gaussian basis sets for use in correlated molecular calculations. V. Core-valence basis sets for boron through neon. J Chem Phys 1995;103:4572–85.
[33] Reiher M, Wolf A. Exact decoupling of the Dirac Hamiltonian. II. The generalized Douglas–Kroll–Hess transformation up to arbitrary order. J Chem Phys 2004;121:10945–56.
[34] De Jong WA, Harrison RJ, Dixon DA. Parallel Douglas–Kroll energy and gradients in NWChem: estimating scalar relativistic effects using Douglas–Kroll contracted basis sets. J Chem Phys 2001;114:48–53.
[35] Berning A, Schweizer M, Werner H-J, Knowles PJ, Palmieri P. Spin-orbit matrix elements for internally contracted multireference configuration interaction wavefunctions. Mol Phys 2000;98:1823–33.
[36] Le Roy RJ. LEVEL: a computer program for solving the radial Schrödinger equation for bound and quasibound levels. J Quant Spectrosc Radiat Transfer 2017;186:167–78.
[37] Qin Z, Zhao J, Liu L. Radiative transition probabilities between low-lying electronic states of N_2. Mol Phys 2019;117:2418–33.
[38] Qin Z, Zhao J, Liu LH. Theoretical study on low-lying electronic states of CP radical: energy levels, Einstein coefficients, Franck-Condon factors and radiative lifetimes. J Quant Spectrosc Radiat Transfer 2019;230:36–47.
[39] NIST. https://physicsnistgov/PhysRefData/ASD/levels_formhtml.
[40] Bauschlicher CW Jr. The convergence of the coupled cluster approach for MgO. Chem Phys Lett 2018;711:27–31.
[41] Huber KP, Herzberg G. molecular spectra and molecular structure: IV constants of diatomic molecules: Von Nostrand-Reinhold. New York: Elsevier; 1979.
[42] Thümmel H, Klotz R, Peyerimhoff SD. Study of the $a^3\Pi$ and $X^1\Sigma^+$ states of the MgO molecule: spin-forbidden transitions and breakdown of the Born-Oppenheimer approximation. Chem Phys 1989;135:229–45.
[43] Bellert D, Burns KL, Van-Oanh N-T, Wang J, Breckenridge W. A new source for vibrationally excited and rotationally cold metal-oxide molecules: spectroscopic characterization of the low-lying $a^3\Pi_2$ metastable excited state of the MgO molecule. Chem Phys Lett 2003;381:381–4.
[44] Büsener H, Heinrich F, Hese A. Electric dipole moments of the MgO $B^1\Sigma^+$ and $X^1\Sigma^+$ states. Chem Phys 1987;112:139–46.
[45] de Vivie R, Marian CM, Peyerimhoff SD. Spin-forbidden transitions in the presence of an intersystem crossing: application to the $b^1\Sigma^+$ state in OH^+. Chem Phys 1987;112:349–61.